Evaluation of Solution-Processable Carbon-Based Electrodes for All-Carbon Solar Cells

Marc P. Ramuz,[†,‡] Michael Vosgueritchian,[†,‡] Peng Wei,[†] Chenggong Wang,[§] Yongli Gao,[§] Yingpeng Wu,[⊥] Yongsheng Chen,[⊥] and Zhenan Bao[†,*]

[†]Department of Chemical Engineering, Stanford University, 381 North-South Mall, Stanford, California 94305, United States, [§]Department of Physics and Astrophysics, University of Rochester, Rochester, New York 14627, United States, and [⊥]Institute of Polymer Chemistry, Nankai University, Weijin Road 94, Tianjin 300071, China. [‡]These authors contributed equally to this work.

ABSTRACT

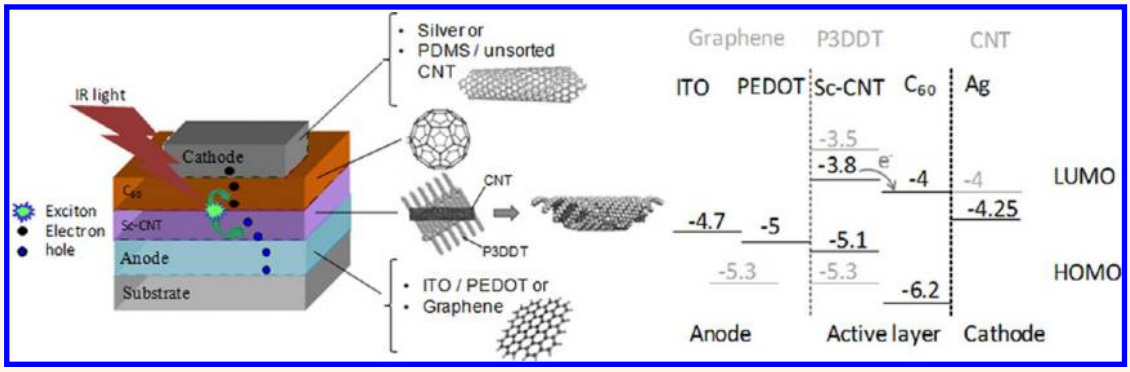

Carbon allotropes possess unique and interesting physical, chemical, and electronic properties that make them attractive for next-generation electronic devices and solar cells. In this report, we describe our efforts into the fabrication of the first reported all-carbon solar cell in which all components (the anode, active layer, and cathode) are carbon based. First, we evaluate the active layer, on standard electrodes, which is composed of a bilayer of polymer sorted semiconducting single-walled carbon nanotubes and C_{60}. This carbon-based active layer with a standard indium tin oxide anode and metallic cathode has a maximum power conversion efficiency of 0.46% under AM1.5 Sun illumination. Next, we describe our efforts in replacing the electrodes with carbon-based electrodes, to demonstrate the first all-carbon solar cell, and discuss the remaining challenges associated with this process.

KEYWORDS: carbon nanotube solar cells · reduced graphene oxide anode · n-type doped carbon nanotube cathode

Carbon is one of the most abundant elements in the earth's crust and is found in many allotropes. The different combinations in which carbon atoms can be arranged produce a wide variety of compounds that have unique and interesting physical, chemical, and electronic properties.[1,2] Carbon allotropes include fullerenes, carbon nanotubes (CNTs), and graphene. Depending on the chemical nature, some have been shown to be conducting, while others are semiconducting. Therefore, it is potentially possible to use these materials in combination to fabricate devices composed completely of carbon-based components. Indeed, carbon-based devices offer several attractive features for use in next-generation electronics. First, due to the abundance of carbon, carbon-based devices can be potentially made cheaply and in large quantities. The production of carbon nanotubes, graphene, and fullerenes has increased exponentially over the past several years, and new methods and processes are continuously being developed to improve upon the scalability and cost.[3,4] Second, these materials can be dispersed and deposited using solution processes, and they are integratable into tools and processes already developed for established materials, such as roll-to-roll manufacturing.[5−7] Third, due to the exceptional electrical and optical properties that can be obtained from these materials, they are highly tunable and can be used in

* Address correspondence to zbao@stanford.edu.

Received for review September 24, 2012 and accepted October 21, 2012.

Published online October 31, 2012
10.1021/nn304410w

many different types of devices such as transistors, solar cells, displays, and supercapacitors.[8−12] Finally, they have long-term chemical and temperature stability potentially unmatched by any other materials.[13−17]

In fact, researchers have already demonstrated all-carbon-based devices, in which both the electrodes and the active components are all made with carbon materials. Jeong *et al*. fabricated an all-carbon nanotube based flexible field emission device.[18] They used a doping strategy to produce both anode and cathode electrodes composed of carbon nanotubes and a carbon nanotube/tetraethylorthosilicate hybrid film as the emitting layer. They illustrated the advantages of using a carbon-based device by demonstrating its high flexibility and environmental stability when compared to devices composed of other materials. All-carbon transistors composed of semiconducting single-walled carbon nanotubes (SWNTs) or graphene nanoribbons with graphene or CNT electrodes and all-carbon supercapacitors have also been demonstrated.[19−22]

More recently, the use of carbon allotropes in photovoltaics has been demonstrated. Fullerenes have been incorporated in organic photovoltaics (OPVs) since 1995.[23,24] Fullerene derivatives, in particular [6,6]-phenyl-C_{61}-butyric acid methyl ester (PC60BM), are the most commonly used acceptor material in OPVs due to their high electron affinity,[25] although there has been a demonstration of using C_{60} as the primary active element in an OPV.[26] Graphene and graphene oxide (GO) have predominately been used in PVs as electrodes and hole transport layers, respectively.[27−32] The thin 2D structure of graphene in addition to its high transparency and conductivity has made it an ideal candidate for electrode material for OPVs. Similarly, CNTs have primarily been used only as electrodes in PVs.[33−36] However, CNTs have also been incorporated in the active layer of solar cells in hybrid structures as an additive to improve charge transport, such as in OPVs,[37−41] silicon PVs,[42,43] and other inorganic PV structures.[44] Recently, Arnold *et al*. reported a solar cell device consisting of an all-carbon active layer with semiconducting nanotubes as both the light-absorbing and donor material with C_{60} as the acceptor. This work demonstrated the potential of carbon-based materials as the primary active elements in a PV.[45,46] Jain *et al*. subsequently produced PVs composed of a single-chirality semiconducting SWNT/C_{60} active layer with a maximum power conversion efficiency (PCE) of 0.1% under AM1.5 100 mW/cm^2 illumination.[47] These devices have active layers that were composed of SWNTs and C_{60}. The single-chirality SWNTs used in this study were dispersed and deposited using a surfactant, which was subsequently removed by rinsing. Tung *et al*. fabricated solar cells with active layers composed of a mixture of solution-processed C_{60}, SWNTs, and reduced graphene oxide. Graphene oxide was used as a surfactant to aid with the dispersion. The maximum PCE of these devices was 0.21% under AM1.5 80 mW/cm^2 illumination and was shown to increase to 0.85% by replacing C_{60} with C_{70}.[48] Despite these advancements toward the production of carbon-based PVs, these devices used standard electrodes, such as indium tin oxide (ITO) as the anode and Ag or Al as the cathode. To date, no all-carbon PV device including both the active layer as well as the electrodes has been fabricated with all-carbon-based materials.

In this work, we report our efforts into the fabrication of an all-carbon PV device: anode, active layer, and cathode. First, we report the optimization of the active layer composed of a bilayer film of a newly reported solution-sorted semiconducting SWNT (as the light absorber and donor) and C_{60} (as the acceptor) on standard electrodes by optimizing the semiconducting SWNT dispersion and deposition conditions and the C_{60} thickness. Next, we report our efforts in replacing the ITO anode with reduced graphene oxide (rGO) layers and the metallic cathode with n-type-doped SWNT films. With the use of these carbon-based electrodes, we demonstrate the first all-carbon-based PV. Finally, we discuss the challenges to be addressed in producing more efficient all-carbon-based PVs.

RESULTS AND DISCUSSIONS

Device Structure. To evaluate the solar cell performance of the carbon active layer, we first used standard electrodes for the device structure as shown in Figure 1. The active layer was composed of a bilayer structure with semiconducting SWNTs as the absorbing and donor layer and C_{60} as the acceptor layer. The semiconducting high-pressure carbon monoxide (HiPCO) SWNTs were sorted using the organic semiconducting polymer regioregular poly(3-dodecylthiophene-2,5-diyl) (P3DDT).[49] We reported previously that regioregular P3DDT can be used to achieve sorting of high-purity semiconducting SWNTs. Both spectroscopic characterizations and electrical characterizations have shown that these polymer-sorted SWNTs were free of metallic SWNTs.[50] In fact, the removal of metallic SWNTs is critical for solar cell devices because their presence would cause shorts and quenching of excitons in the device.

With polymer-free SWNTs, excitons are generated by the SWNTs after absorbing light mostly in the near-infrared (NIR) region, and exciton dissociation occurs at the SWNT/C_{60} interface.[46,51] The electrons and holes are then transported to the cathode and anode, respectively. In our P3DDT-sorted SWNT system, a residue amount of P3DDT is still present in the film even after washing. Unlike previous work in which high band gap polymers composed of fluorene- and carbazole-based homo- and copolymers were used for sorting SWNTs or surfactant dispersed sorted semiconducting SWNTs were used,[52−54] P3DDT has a strong absorption of visible light. Therefore, in this work we

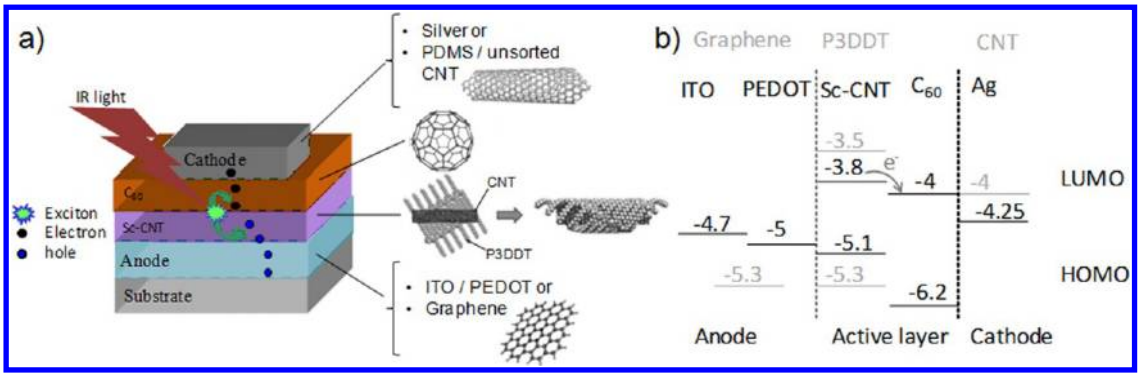

Figure 1. (a) Structure of SWNT-based PV, with ITO/PEDOT or rGO as the anode and Ag or n-type-doped SWNTs as the cathode. (b) Band diagram of the PV device shown in (a). The energy levels for the materials were from literature or our own measurements.[45,55]

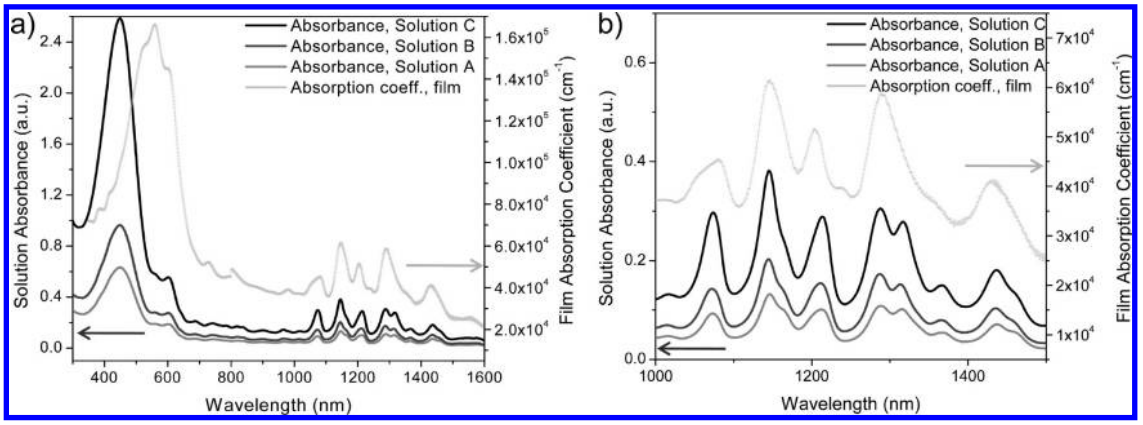

Figure 2. Absorbance spectra and absorption coefficient of SWNTs wrapped by P3DDT at different concentrations (a) in the range 300−1600 nm and (b) in the range 1000−1500 showing individual SWNT peaks. All solutions were made by sonicating 10 (solution A), 20 (solution B), and 30 mg (solution C) each of P3DDT and SWNT in 25 mL of toluene followed by centrifugation to remove undispersed SWNTs. The SWNT film was made by spray coating solution B onto a glass substrate. The absorption coefficient was measured for a film on a glass substrate. All other curves are from solution.

compared the results with both full-Sun and NIR illumination.

In the standard electrode structure, the anode was composed of an ITO with a poly(3,4-ethylenedioxythiophene):poly(styrenesulfonate (PEDOT:PSS) layer as a hole-transporting layer and Ag as the cathode. On each glass substrate, 6 pixels with an area of 4 mm^2 were fabricated. The results shown in this work are the average values of these pixels, except where noted. The current−voltage (I−V) measurements were performed using a solar simulator (see Materials and Methods for more details). Both full spectra and ones with an optical filter that cut off light with wavelengths below 800 nm were obtained. In the filtered case, the photogenerated charges from P3DDT were negligible because P3DDT does not absorb at wavelengths above 800 nm. For the all-carbon device discussed later, thermally reduced graphene oxide was used for the anode instead of ITO/PEDOT, and n-type doped unsorted SWNTs for the cathode instead of Ag.

Optical Properties of the SWNT Layer. The deposited SWNT films showed high absorption in the NIR region, up to 1500 nm (Figure 2). This indicates the promise of these films as IR absorbers for PVs, which can complement other PV materials that absorb poorly in the NIR region. Indeed the use of SWNTs for NIR photodetectors has been reported by other researchers.[46,54,56] The absorption range of SWNTs is highly dependent on the type (diameter and chirality) of the SWNTs, which is determined by the SWNT synthesis and sorting process.[57,58] Therefore, the incorporation of a broader range of different types of semiconducting SWNTs would potentially further increase the absorption range of these devices, and thus the efficiency. It should be noted that the peak absorbance of the SWNT films overlaps better with the sun spectrum than with the peaks in the light output of our solar simulator, which limited the absorption of the SWNT layer and reduced the achievable efficiency using the current standard setup (see Supporting Information for more details).

To increase the absorbance of the SWNT layer, several different concentrations of the P3DDT-sorted SWNT dispersions were prepared to obtain different SWNT thicknesses while keeping the P3DDT:SWNT weight ratio the same at 1:1. Figure 2a shows the absorbance spectra for devices made with solutions

of 10 (solution A), 20 (solution B), and 30 mg (solution C) each of P3DDT and SWNT sonicated in 25 mL of toluene followed by centrifugation to remove undispersed SWNTs. The absorption peak in the 350−650 nm range was from the P3DDT, and the smaller peaks in the 1050−1500 nm range were from the SWNTs, with each peak corresponding to a different SWNT chirality. The detailed analysis of the chirality of the SWNTs present was presented previously.[49] The majority of the SWNTs were (12,1), (10,5), (8,6), (9,4), and (9,5). As seen in Figure 2b, the nanotube peak absorption coefficient, from spray-coated solution B on a glass substrate, was measured to be 6×10^4 cm^{-1}, which is lower than that of P3DDT absorbance in the same film in the visible range (1.6×10^5 cm^{-1}) but is remarkable for the NIR range compared to typical organic solar cell materials, which normally do not absorb much in the NIR. Moreover, by increasing the SWNT density, higher absorption coefficients should be possible. The absorption peaks in the 400−600 nm region are from the P3DDT polymer. As observed in our previous work, typically the P3DDT solution has a single absorption peak at ~450 nm; however, an additional peak is observed when it is dispersed with the SWNTs at ~600 nm, which has been attributed to the polymer/SWNT interaction.[49]

Photovoltaic Performance. Photovoltaic devices were first made using the P3DDT/SWNT dispersions with ITO/PEDOT as the anode and Ag as the cathode. The current−voltage ($I-V$) curves and PV performance of these devices are shown in Figure 3 and Table 1, respectively. As expected, the short-circuit current (J_{sc}) increased with increasing SWNT concentration, which was due to increased light absorption, and thus increased exciton generation, in these layers (Figure 2). The ratio between the current under illumination and in the dark (on/off ratio at 0 V) increased from 480 to 3180 for the low-concentration solution A (10 mg/25 mL toluene) to high-concentration solution C (30 mg/25 mL toluene). Solutions with even higher concentrations were attempted (40 mg/25 mL toluene) but failed because the P3DDT was not able to disperse the SWNTs at such a high concentration. All devices hereafter were made with solution C.

In addition to increasing the SWNT concentration to vary the SWNT layer thickness, different deposition conditions were attempted to further increase the overall absorption and performance of the devices. To obtain thicker layers, multiple layers were spin-coated in addition to drop casting the films. To obtain a thick film with a good uniformity, the minimum spin-coating speed possible was 300 rpm for 90 s. After annealing these films to remove the solvent, the process was repeated three and five times, respectively. Film thicknesses of 3, 4, and 5.5 nm were obtained for one-, three-, and five-layer spin-coating, respectively. The absorption spectra of these films are shown in Figure 4, and the PV performance is shown in Table 2. As expected, the J_{sc} and the efficiency increased with increased layer thickness, as the SWNT became thicker and absorbed more light. The drop-casted films were much thicker, *ca.* 25−100 nm, but did

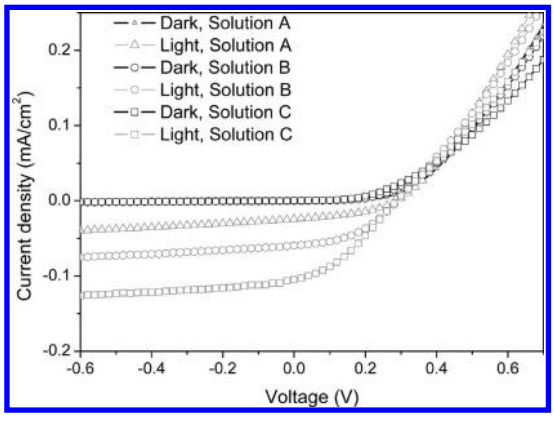

Figure 3. $I-V$ characteristics of PV devices under IR illumination with different SWNT concentrations.

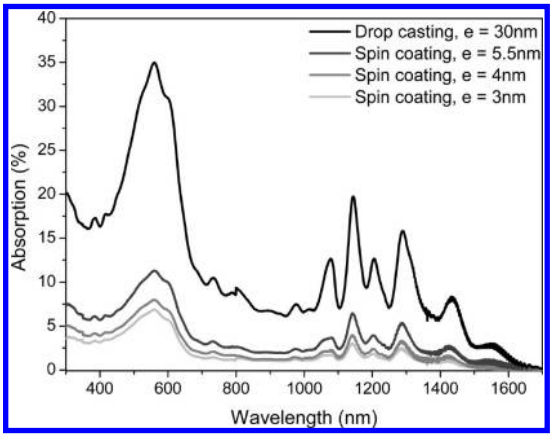

Figure 4. Absorption spectra of PV devices made with different deposition conditions with a 30 mg/25 mL toluene solution.

TABLE 1. PV Characteristics for Devices with Different SWNT Concentrations for NIR Illumination and under Standard Illumination AM1.5 100 mW/cm^2 [a]

				NIR illumination			AM1.5	
solution	J_{sc} (mA/cm^2)	V_{oc} (V)	FF	on/off @ 0 V	av PCE (%)	max PCE (%)	av PCE (%)	max PCE (%)
solution A	-2.29×10^{-2}	0.28	0.403	480	5.62×10^{-3}	6.35×10^{-3}	2.28×10^{-1}	2.40×10^{-1}
solution B	-6.20×10^{-2}	0.29	0.436	1996	1.73×10^{-2}	2.04×10^{-2}	2.34×10^{-1}	2.38×10^{-1}
solution C	-1.13×10^{-1}	0.29	0.348	3180	2.54×10^{-2}	2.79×10^{-2}	1.80×10^{-1}	1.84×10^{-1}

[a] The data correspond to five devices per solution.

TABLE 2. PV Characteristics of a Device Made with Different Deposition Conditions with Solution C (30 mg/25 mL) for NIR Illumination and under Standard Illumination AM1.5 100 mW/cm^2[a]

	NIR illumination						AM1.5	
deposition/thickness	J_{sc} (mA/cm^2)	V_{oc} (V)	FF	on/off @ 0 V	av PCE (%)	max PCE (%)	av PCE (%)	max PCE (%)
spin coat 1×/3 nm	-9.92×10^{-2}	0.30	0.43	2395	2.85×10^{-3}	3.82×10^{-2}	0.184	0.191
spin coat 3×/3 nm	-1.29×10^{-1}	0.31	0.41	2707	3.65×10^{-2}	2.04×10^{-2}	0.174	0.177
spin coat 5×/3 nm	-1.48×10^{-1}	0.30	0.40	3054	4.00×10^{-2}	4.32×10^{-2}	0.175	0.179
drop cast/25−100 nm	-1.41×10^{-1}	0.30	0.39	18910	3.56×10^{-2}	4.24×10^{-2}	0.125	0.140

[a] The data correspond to five devices per deposition condition with a 140 nm C_{60} layer.

not show improved J_{sc} when compared to the devices with five spin-coated layers. In addition, thicker layer spin-coated film (>5 spin-coated layers) did not show further improvement. Both these results are likely due to the short exciton diffusion length in our system. Even though the exciton diffusion length has been shown to be ~100 nm within an individual SWNT,[59,60] Arnold *et al.* have shown that the exciton diffusion length in SWNT networks is only ~5 nm because of poor exciton hopping ability between SWNTs.[45,46] Our observations that thicker films than 5 nm did not show improved J_{sc} are consistent with the poor exciton diffusion hypothesis proposed by others. In addition, thicker films showed lower fill factor (FF) values (decreasing the overall efficiency of the PV devices), which was attributed to nonuniformity of the films and a greater tendency for exciton recombination.

C_{60} Thickness Optimization. The C_{60} acceptor layer thickness also has a significant effect on the device performance. This n-type layer was deposited *via* vacuum thermal evaporation (see Materials and Methods for more information). Thicknesses ranging from 40 to 190 nm, as measured by a quartz crystal monitor during deposition, were evaluated while keeping the thickness of the SWNT layer constant (3 nm) with an ITO/PEDOT anode and an Ag cathode. A plot of the PCE *versus* C_{60} thickness is shown in Figure 5. For a C_{60} film of 40 nm, the performance was poor, as evident by a low open circuit voltage (V_{oc}) due to device shorting as a result of insufficient C_{60} coverage. AFM images (Figure 6) confirmed exposed SWNTs on the surface when a thin layer of C_{60} film was deposited. By increasing the C_{60} thickness, the SWNTs were fully covered, and the V_{oc} and FF improved. We attribute the high thickness needed to cover the relatively thin SWNT layers to the 3D growth mechanism of C_{60}, as has been observed previously.[61,62] As seen in Figure 5, the PCE and current density showed the highest values for C_{60} at thicknesses of both 80 and 140 nm. As already reported, this may be attributed to constructive interference of a cavity effect formed by the Ag cathode acting as a mirror for the incoming light that is not absorbed by the active layer.[63] For a C_{60} thickness higher than 160 nm, the current density, and therefore the PCE, decreased drastically due to resistive losses during the transport of electrons in the C_{60} layer.

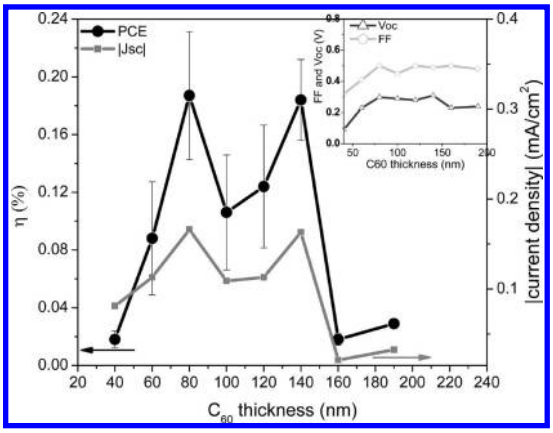

Figure 5. Influence of the C_{60} thickness on the device performance. The main plot shows the power conversion efficiency (with the standard deviation) and the absolute value of the short-circuit current as a function of C_{60} thickness. The inset shows the V_{oc} and FF as a function of C_{60} thickness.

Based on the optimized SWNT and C_{60} layer thickness with ITO/PEDOT anode benzocyclobutene (BCB)/Ag cathode, the best device we obtained gave a maximum PCE of 0.13% in the NIR (incoming light filtered below 800 nm) and 0.46% for AM1.5 Sun 100 mW/cm^2 illumination, respectively (Figure 7). The increased PCE for the AM1.5 Sun illumination compared to the NIR illumination is due to the increased absorption due to the C_{60} and P3DDT, as evident by a 4-fold increase in the J_{sc}. The external quantum efficiency (EQE) was measured for the optimized device structure (see Materials and Methods section and Supporting Information for more information) and showed a peak of 5% at 1150 nm. These results are comparable to the previously mentioned SWNT/fullerene-based solar cells with an ITO/PEDOT anode and metallic cathode, where maximum PCEs in the range 0.1−0.85% were demonstrated.[45−48] It should be noted that our system may form a type II heterojunction due to the P3DDT/SWNT interaction. The type II heterojunction is defined as the heterojunction formed due to the interaction between the holes in the valence band of the SWNT and the highest occupied molecular orbital (HOMO) of the P3DDT, which can have an impact on the exciton dissociation process.[64,65] Further work is under way to understand the role of the P3DDT polymer in our system.

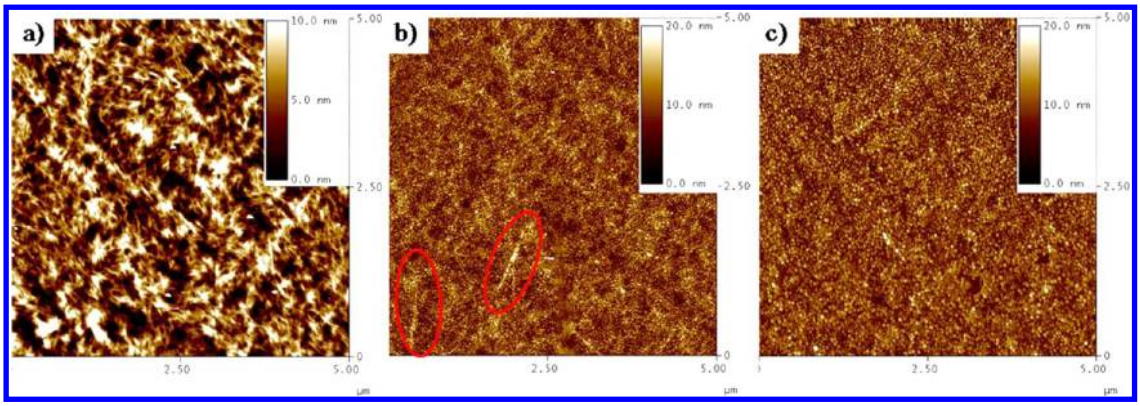

Figure 6. AFM images of (a) SWNT active layer, (b) 80 nm of C_{60} on top of the SWNT layer showing protruding SWNTs, and (c) 120 nm of C_{60} on SWNTs showing complete coverage.

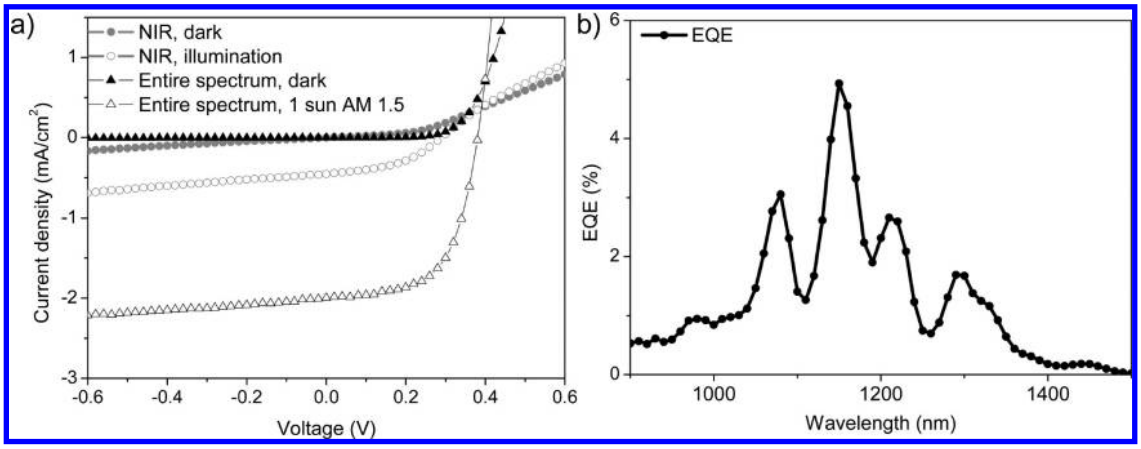

Figure 7. (a) *I*–*V* characteristic of the optimized devices measured under standard illumination AM1.5 (dark lines) and under NIR illumination (gray lines), which show power conversion efficiencies of 0.46% (J_{sc} = 2.00 mA/cm^2, V_{oc} = 0.39, FF = 0.59) and 0.13% (J_{sc} = 0.453 mA/cm^2, V_{oc} = 0.31, FF = 0.51), respectively. (b) EQE of the optimized device in the NIR region.

Carbon-Based Electrodes for All-Carbon Device Structure. This section discusses our efforts in replacing the ITO anode and the Ag cathode with carbon electrodes, using rGO and n-doped SWNTs, to fabricate a PV device composed entirely of carbon-based materials. To the best of our knowledge, this structure is the first demonstration of an all-carbon-based solar cell (anode, active layer, and cathode).

Much work has been focused on replacing ITO as the anode in conventional organic PVs because the indium-containing ITO is both brittle and expensive.[66,67] Some of the materials used thus far include graphene,[32,68,69] CNTs,[35,70] silver and copper nanowires,[71,72] patterned metal grids,[73,74] and organic polymers (PEDOT).[75–77] These alternative materials have also produced flexible devices. In fact, Zhou *et al.* fabricated a flexible organic PV consisting of PEDOT as both the anode and the cathode using a doping strategy.[78] In our group, we have demonstrated the first stretchable organic PV by using PEDOT on a buckled polydimethylsiloxane (PDMS) substrate as the anode and EGaIn as the cathode.[79] Flexible and stretchable graphene and carbon nanotube electrodes have also been demonstrated, illustrating their use in flexible and stretchable electronics.[80–82] In contrast, less effort and progress have been made into replacing the metallic cathodes in PVs; however, it would be advantageous to do so to increase the flexibility and the overall transparency of the device. In fact, Liu *et al.* used a combination of graphene and PEDOT to fabricate a semitransparent organic PV.[83] Other demonstrations of replacing the metallic cathode with alternative materials can be found as well.[84–87]

In our all-carbon PV devices, we used rGO as the anode and n-type-doped SWNTs as the cathode (Figure 1a). The rGO anodes were fabricated using a thermal reduction method previously developed in our group.[88] A graphene electrode was chosen (instead of CNTs) due to the smooth films that can be formed, thus reducing the amount of leakage and the possibility of shorting in the device. Recently, researchers have successfully used graphene-based electrodes in light-emitting diodes as a replacement for ITO.[89,90] In addition, rGO films were chosen instead of transferred CVD films of graphene because devices made using transferred CVD graphene exhibited high leakage or

shorting. We attributed this result to roughness problems associated with residue contamination caused by the transfer process, as has been observed in the literature.[91,92] Although the rGO films are less conductive (and less transparent) than transferred CVD films, the resulting devices were better performing due to the smoothness of the films. To increase the work-function of the rGO films, they were treated with short periods of O_2 plasma (5−10 s), which resulted in a work-function increase from 4.9 eV to 5.3 eV (see Supporting Information for more details on work-function results and measurements).[93] AFM images of the graphene before and after O_2 treatment are shown in Figure 8a and b, respectively. After the O_2 plasma treatment, the SWNT/P3DDT and C_{60} layers were deposited in the same manner as described in earlier sections.

To evaluate the effectiveness of the rGO electrode, devices were fabricated with the rGO anode and the standard Ag cathode. In addition to rGO anodes with plasma, devices were fabricated with an additional PEDOT smoothening layer. The PV performances for these devices are summarized in Table 3. As can be seen, the devices with an rGO anode and Ag cathode resulted in decreased V_{oc} and FF compared to the ITO/PEDOT anode, with an associated decrease in the PCE. The best device with this structure had a PCE of 0.14% for AM1.5 Sun illumination. Also, the device to device variation was greater. We attributed both these results to the increased roughness of the rGO when compared to the ITO anode. This effect was further verified by the addition of a planarizing and high-conductivity PEDOT layer, which significantly improved device performance. Additionally, the high sheet resistance of these films (2−4 kΩ/□ at ∼85% transparency in the visible) resulted in lower device performance due to resistive loss during charge collection.

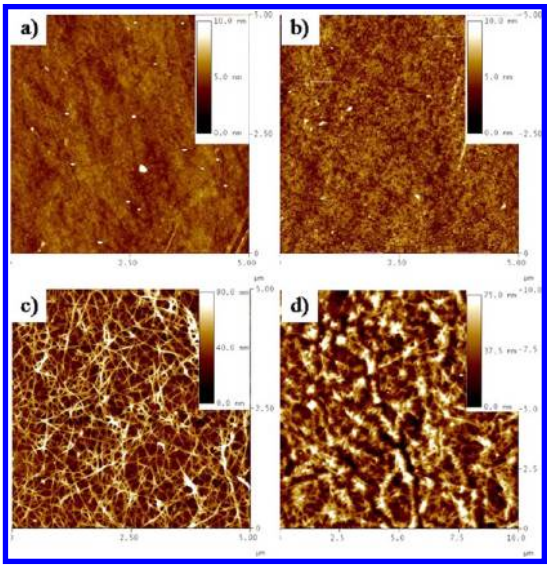

Figure 8. AFM images of (a) rGO films, (b) rGO film after plasma treatment, (c) spry-coated SWNT film on PDMS, and (d) SWNT films on PDMS after n-type doping.

The SWNT cathodes were fabricated by spray-coating a solution of SWNTs (1/3 metallic) dispersed in *N*-methyl-2-pyrrolidone (NMP) on polydimethylsiloxane substrates (see Materials and Methods section for details). These films were then doped as n-type using the molecular n-type dopant (4-(1,3-dimethyl-2,3-dihydro-1*H*-benzoimidazol-2-yl)phenyl)dimethylamine (N-DMBI) (see Materials and Methods section for doping details), which we have previously reported to dope C_{60} and PCBM.[94,95] After doping, the sheet resistances of these films were 200−300 Ω/□ (70−80% transmittance in the visible). The work-function measured by ultraviolet photoemission spectroscopy was −3.4 to −4.24 eV depending on the amount of dopants applied, making them suitable as the cathode material (more information on the work-function measurements are provided in the Supporting Information). A SWNT-based film was used as the cathode because of the ease of its solution processability and readily tunable electronic property by the efficient n-type doping.[80] AFM images of the SWNT cathode films before and after doping are shown in Figure 8c and d, respectively. After completion, these films were laminated on the rGO/SWNT:P3DDT/C_{60} layers by pressing the films together.

To evaluate the effect of the n-type-doped SWNT cathode, it was laminated on devices fabricated on the

TABLE 3. PV Characteristics of Devices Made with rGO Anodes with Ag Cathodes, ITO Anodes with n-Type-Doped SWNT Cathodes, and rGO Anodes with n-Type-Doped SWNT Cathodes, for NIR Illumination and under Standard Illumination AM1.5 100 mW/cm^2 [a]

	NIR illumination						AM1.5	
anode/cathode	J_{sc} (mA/cm^2)	V_{oc} (V)	FF	on/off @ 0 V	av PCE (%)	max PCE (%)	av PCE (%)	max PCE (%)
rGO-plasma/Ag	-2.84×10^{-2}	0.25	0.52	1731	8.16×10^{-3}	8.16×10^{-3}	1.41×10^{-1}	1.41×10^{-1}
rGO-PEDOT/Ag	-4.51×10^{-2}	0.26	0.50	1035	1.31×10^{-2}	2.01×10^{-2}	2.36×10^{-1}	2.69×10^{-1}
ITO/n-doped SWNTs	-2.79×10^{-1}	0.08	0.25	30	1.29×10^{-2}	1.46×10^{-2}	2.49×10^{-1}	3.04×10^{-1}
rGO-plasma/n-doped SWNTs	-3.00×10^{-2}	0.18	0.28	1607	3.42×10^{-3}	4.10×10^{-3}	4.71×10^{-3}	5.67×10^{-3}

[a] It should be noted that not all devices fabricated using rGO anodes were successful because of large graphitic-like particulates that were formed during the rGO film fabrication step. The data correspond to 1, 3, 3, and 3 devices for the different anode/cathode combinations from top to bottom.

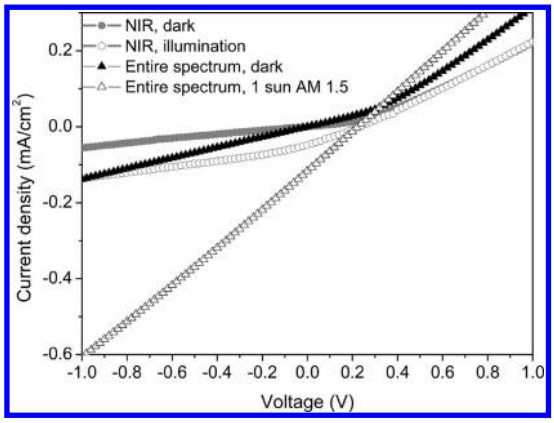

Figure 9. *I*–*V* characteristics of all-carbon devices with an rGO anode and n-type-doped laminated SWNT cathode. The active layer was composed of a 5 nm layer of semiconducting sorted SWNTs and 130 nm C_{60}. The device areas were ~0.015 cm^2.

standard ITO anode. The PV performance of these devices is summarized in Table 3. As can be seen, there was a significant decrease in the V_{oc} for these devices and a marginal decrease in the FF and J_{sc}, which decreased the overall PCE. The best device with this structure had a PCE of 0.015% in the NIR range and 0.3% under AM1.5 Sun. We attributed the large decrease in V_{oc} for the NIR range due to contact issues between the laminated SWNT cathode and the C_{60} because of the high roughness of the SWNT cathode. Additionally, as mentioned earlier, the light intensity in the NIR range from the solar simulator is relatively low, which might also reduce the V_{oc}.[96] Efforts to directly deposit the n-type-doped SWNTs on the C_{60} failed because the NMP solvent damaged the underlying films.

Finally, all-carbon devices were fabricated using the rGO anodes and n-type-doped SWNT cathodes. The device yield was low due to shorting or high leakage. We attributed this to roughness and contamination issues in the rGO films compounded by the lamination process of the high roughness n-type-doped SWNT films. Nevertheless, working devices were fabricated with the all-carbon structure as shown in Figure 1a. Figure 9 shows the typical *I*–*V* characteristics and device performance of the fabricated all-carbon solar cells. The best all-carbon devices fabricated had a PCE of 4.1×10^{-3} % and 5.7×10^{-3} % under NIR and standard AM1.5 illuminations, respectively. Contrary to devices with standard electrodes (ITO and Ag), the increase in light intensity under AM1.5 illumination only increased slightly the current in the output circuit, which was due to the losses at the electrodes, which we attributed to contact resistance between the electrodes and the active layer.

Summary and Outlook on All-Carbon Solar Cells. In this report, we have described our efforts into the fabrication of an all-carbon solar cell. By optimizing the active layer thickness, which was composed of semiconducting sorted SWNTs wrapped by P3DDT and a C_{60} layer, on standard electrodes (ITO and Ag) we were able to obtain devices with a PCE of 0.13% in the NIR range and 0.46% under standard illumination AM1.5, comparable to that reported for polyfluorene-sorted SWNTs. Upon replacing one of the standard electrodes with carbon electrodes by using either rGO for the anode or n-type-doped SWNTs as the cathode in conjunction with standard cathode or anode, respectively, only a small degradation of the AM1.5 Sun performance was seen. This shows the potential of carbon electrodes for all-carbon solar cells. Combining the rGO anode and doped SWNT cathode, we were able to fabricate the first all-carbon solar cell, which had a PCE of 4.1×10^{-3} % for NIR illumination. We believe that by overcoming some of the challenges described in this work for all-carbon devices, the PCE can be significantly increased.

For the active layer, the absorption can be increased by introducing other types of semiconducting SWNTs that absorb in a broader range of the solar spectrum. For example, larger diameter tubes, such as those grown by the arc-discharge method, would greatly enhance the amount of absorption especially between 900 and 1200 nm. Additionally, changing the device structure of the randomly aligned SWNT layer to a unidirectionally aligned structure in which individual SWNTs can directly bridge the electrodes would greatly reduce the exciton trapping by tube-to-tube junctions and increase the exciton diffusion length in the system.[47]

Significant improvements need to be made to the carbon electrodes. With respect to the rGO anode, the replacement of this layer with a smoother and more conductive graphene film would significantly enhance the charge collection and device reproducibility. Care should be taken to limit the amount of contamination or residue left behind during the fabrication of this layer. Also, the rGO layer used in this system has a relatively low transparency, 80–85% in the visible and ~85% in the NIR (see Supporting Information for more details). As a result, a lower light intensity also contributed to the lower performance. For the cathode, the fabrication of a smooth SWNT film with better contact to the active layer would significantly improve device performance. The challenge is to directly fabricate the SWNT cathode on the semiconducting SWNT and C_{60} active layer without damaging the underlying active layer. In addition, because SWNTs do not reflect light, there are no constructive interference effects of the transmitted light compared to a highly reflective metallic cathode.

Finally, as previously mentioned, it should be noted that the peak absorbance of the SWNT films in our system does not have good overlap with the light output of our solar simulator, which limited the absorption of the SWNT layer and reduced the achievable

efficiency using the current standard setup (see Supporting Information for more details). We anticipate that with all the above improvements to the device, all-carbon solar cells with PCE of >1% should be possible.

MATERIALS AND METHODS

Semiconducting SWNT Solution and Film Fabrication. The details of the sorting process can be found elsewhere.[49] Briefly, commercially available HiPCO SWNTs (Unidym) and P3DDT (regioregular, Sigma-Aldrich) at varying concentrations were sonicated in toluene, in an acetone bath, using a tip-sonicator (Ultrasonic Processor, Cole Palmer) at 70% power for 1 h. The solution was then centrifuged for 1.5 h at 17 000 rpm to remove the SWNT bundles, undispersed carbon, and other contaminants. The upper 75% of the resulting solution in the centrifugation tube was decanted and spin-coated on the desired anode using the following conditions: 0 rpm for 1 min, 300 rpm for 1 min, and 1200 rpm for 10 s. The substrates were then annealed on a hot plate at 100 °C for 5 min.

C_{60} and Ag Deposition. Commercially available C_{60} (Fullerene Powder, sublimed, 99.9+%, Alfa Aesar) was deposited thermally under vacuum (5×10^{-5} Torr) at 0.05 nm/s (Angstrom Engineering evaporator). Similarly, Ag was vacuum evaporated on top of the C_{60} at 0.05 nm/s (Thermionics Laboratory, Inc. evaporator).

rGO Anode Fabrication. The details of the rGO layer fabrication can be found elsewhere.[88] Briefly, commercially available graphene oxide was bath sonicated in water for 3 h at 60 °C, followed by centrifugation for 30 min at 14 000 rpm to remove the undispersed GO. The top 75% of the solution was decanted and spin-coated on quartz slides (2.0 cm × 2.5 cm) at 1000 rpm for 1 min. The substrates were then annealed on a hot plate at 100 °C for 1 h. The dried substrates were placed in a quartz boat with one end closed (1 in. diameter, 3 feet long). The tube was placed into a Lindberg/BlueM split hinge oven (Lindberg/Blue M 3-zone tube oven, Blue-M), and the open end was fitted to a turbo-pump vacuum line (Turbo-V 250 MacroTorr, Varian Inc.). The oven was heated to 100 °C at ambient pressure; then, the turbo pump was switched on, and a vacuum of 10^{-4} Torr was established before increasing the temperature to 1100 °C at a rate of 20 °C/min. The temperature was held constant for 3 h, after which the oven was allowed to cool for 3 h before removing the samples.

n-Type-Doped SWNT Cathode Fabrication. Commercially available arc-discharged SWNTs (ASP-100F, Hanwan Nanotech) were sonicated in NMP (Sigma-Alrdrich), in an ice water bath, using a tip-sonicator at 30% power for 30 min. The solution was then centrifuged for 45 min at 8000 rpm to remove large bundles and other contaminants. The upper 75% of the resulting solution was decanted and spray coated, using a commercial airbrush (Master Airbrush, model SB844-SET), on PDMS substrates (2 cm × 2.5 cm). The substrates were first activated with UV-ozone for 15 min, then held at 180 °C on a hot plate, and the nanotubes were sprayed at a distance of ~10 cm using an airbrush pressure of 35 psi. The substrates were made by puddle-casting a mixed and degassed PDMS prepolymer (Dow Corning Sylgard 184, with a ratio of base to cross-linker of 10:1 by mass) against the polished surface of a silicon wafer followed by curing at 60 °C for at least 30 min. Once the substrates were cooled to room temperature, they were transferred to a N_2-filled glovebox to be doped by the n-type dopant. N-DMBI in ethanol solutions with different concentrations were spin-coated onto the substrates with the same volume (80 μL) inside the glovebox. After doping, they were laminated on top of a C_{60} layer using alligator clips.

Characterization. AFM images were taken using tapping mode (light tapping regime) using a Multimode AFM (Veeco). Solar spectrum measurements were taken with a Newport solar simulator with a flux of 100 mW/cm^2 that approximated the solar spectrum under AM1.5G conditions. A filter (FGL780S, Thorlabs Inc.) was applied to cut light below 800 nm for NIR measurements (see Supporting Information for more details). We measured the current density *vs* voltage in a N_2 glovebox in the dark and under illumination using a Keithley 2400 Sourcemeter and collected the data electronically using a custom LabView script. Sheet resistance measurements were taken using van der Pauw method with four colinear probes connected to a Keithley 2400 Sourcemeter. Optical-transmission measurements (UV−vis) were taken using a Cary 6000i spectrophotometer.

Conflict of Interest: The authors declare no competing financial interest.

Acknowledgment. The authors would like to thank the Global Climate and Energy Project (GCEP) at Stanford University and the Air Force Office for Scientific Research (FA9550-12-1-01906) for funding.

Supporting Information Available: Details on the solar spectrum filtering, comparison of SWNT absorption to solar spectrum intensity, EQE measurement details and full EQE spectrum, work-function measurements, UV−vis spectra of the rGO and n-type-doped SWNT electrodes, and full PV characteristics for both NIR and standard 1.5AM illumination can be found. This material is available free of charge *via* the Internet at http://pubs.acs.org.

REFERENCES AND NOTES

1. Hirsch, A. The Era of Carbon Allotropes. *Nat. Mater.* **2010**, *9*, 868–871.
2. Dinadayalane, T.; Leszczynski, J. Remarkable Diversity of Carbon−Carbon Bonds: Structures and Properties of Fullerenes, Carbon Nanotubes, and Graphene. *Struct. Chem.* **2010**, *21*, 1155–1169.
3. Noorden, R. V. Chemistry: The Trials of New Carbon. *Nature* **2011**, *469*, 14–16.
4. Murayama, H.; Tomonoh, S.; Alford, J. M.; Karpuk, M. E. Fullerene Production in Tons and More: From Science to Industry. *Fullerenes, Nanotubes, Carbon Nanostruct.* **2005**, *12*, 1–9.
5. Premkumar, T.; Mezzenga, R.; Geckeler, K. E. Carbon Nanotubes in the Liquid Phase: Addressing the Issue of Dispersion. *Small* **2012**, *8*, 1299–1313.
6. Lee, C. W.; Han, X.; Chen, F.; Wei, J.; Chen, Y.; Chan-Park, M. B.; Li, L.-J. Solution-Processable Carbon Nanotubes for Semiconducting Thin-Film Transistor Devices. *Adv. Mater.* **2010**, *22*, 1278–1282.
7. Bae, S.; Kim, H.; Lee, Y.; Xu, X.; Park, J.-S.; Zheng, Y.; Balakrishnan, J.; Lei, T.; Ri Kim, H.; Song, Y. I.; *et al.* Roll-to-Roll Production of 30-Inch Graphene Films for Transparent Electrodes. *Nat. Nanotechnol.* **2010**, *5*, 574–578.
8. Baughman, R. H.; Zakhidov, A. A.; de Heer, W. A. Carbon Nanotubes−the Route toward Applications. *Science* **2002**, *297*, 787–792.
9. Schnorr, J. M.; Swager, T. M. Emerging Applications of Carbon Nanotubes. *Chem. Mater.* **2011**, *23*, 646–657.
10. Geim, A. K. Graphene: Status and Prospects. *Science* **2009**, *324*, 1530–1534.
11. Geim, A. K.; Novoselov, K. S. The Rise of Graphene. *Nat. Mater.* **2007**, *6*, 183–191.
12. Prato, M. [60]Fullerene Chemistry for Materials Science Applications. *J. Mater. Chem.* **1997**, *7*, 1097–1109.
13. Yu, M.-F.; Lourie, O.; Dyer, M. J.; Moloni, K.; Kelly, T. F.; Ruoff, R. S. Strength and Breaking Mechanism of Multiwalled Carbon Nanotubes under Tensile Load. *Science* **2000**, *287*, 637–640.
14. Mohamed, A. O.; Srivastava, D. Temperature Dependence of the Thermal Conductivity of Single-Wall Carbon Nanotubes. *Nanotechnology* **2001**, *12*, 21.
15. Lee, C.; Wei, X.; Kysar, J. W.; Hone, J. Measurement of the Elastic Properties and Intrinsic Strength of Monolayer Graphene. *Science* **2008**, *321*, 385–388.
16. Amanda, S. B. Modelling the Relative Stability of Carbon Nanotubes Exposed to Environmental Adsorbates and Air. *J. Phys.: Condens. Matter* **2009**, *21*, 144205.

17. Gao, D.; Helander, M. G.; Wang, Z.-B.; Puzzo, D. P.; Greiner, M. T.; Lu, Z.-H. C60:Lif Blocking Layer for Environmentally Stable Bulk Heterojunction Solar Cells. *Adv. Mater.* **2010**, *22*, 5404–5408.
18. Jeong, H. J.; Jeong, H. D.; Kim, H. Y.; Kim, J. S.; Jeong, S. Y.; Han, J. T.; Bang, D. S.; Lee, G.-W. All-Carbon Nanotube-Based Flexible Field-Emission Devices: From Cathode to Anode. *Adv. Funct. Mater.* **2011**, *21*, 1526–1532.
19. Jang, S.; Jang, H.; Lee, Y.; Suh, D.; Baik, S.; Hong, B. H.; Ahn, J.-H. Flexible, Transparent Single-Walled Carbon Nanotube Transistors with Graphene Electrodes. *Nanotechnology* **2010**, *21*, 425201.
20. Li, B.; Cao, X.; Ong, H. G.; Cheah, J. W.; Zhou, X.; Yin, Z.; Li, H.; Wang, J.; Boey, F.; Huang, W.; *et al*. All-Carbon Electronic Devices Fabricated by Directly Grown Single-Walled Carbon Nanotubes on Reduced Graphene Oxide Electrodes. *Adv. Mater.* **2010**, *22*, 3058–3061.
21. Kaempgen, M.; Chan, C. K.; Ma, J.; Cui, Y.; Gruner, G. Printable Thin Film Supercapacitors Using Single-Walled Carbon Nanotubes. *Nano Lett.* **2009**, *9*, 1872–1876.
22. Lee, S.-K.; Jang, H. Y.; Jang, S.; Choi, E.; Hong, B. H.; Lee, J.; Park, S.; Ahn, J.-H. All Graphene-Based Thin Film Transistors on Flexible Plastic Substrates. *Nano Lett.* **2012**.
23. Yu, G.; Gao, J.; Hummelen, J. C.; Wudl, F.; Heeger, A. J. Polymer Photovoltaic Cells: Enhanced Efficiencies *Via* a Network of Internal Donor-Acceptor Heterojunctions. *Science* **1995**, *270*, 1789–1791.
24. Sariciftci, N. S.; Braun, D.; Zhang, C.; Srdanov, V. I.; Heeger, A. J.; Stucky, G.; Wudl, F. Semiconducting Polymer-Buckminsterfullerene Heterojunctions: Diodes, Photodiodes, and Photovoltaic Cells. *Appl. Phys. Lett.* **1993**, *62*, 585–587.
25. Scharber, M. C.; Mühlbacher, D.; Koppe, M.; Denk, P.; Waldauf, C.; Heeger, A. J.; Brabec, C. J. Design Rules for Donors in Bulk-Heterojunction Solar Cells—Towards 10% Energy-Conversion Efficiency. *Adv. Mater.* **2006**, *18*, 789–794.
26. Chen, L. J.; Song, Q. L.; Xiong, Z. H.; Huang, J. H.; He, F. Environment-Friendly Energy from All-Carbon Solar Cells Based on Fullerene-C60. *Sol. Energy Mater. Sol. Cells* **2011**, *95*, 1138–1140.
27. Hsu, C.-L.; Lin, C.-T.; Huang, J.-H.; Chu, C.-W.; Wei, K.-H.; Li, L.-J. Layer-by-Layer Graphene/Tcnq Stacked Films as Conducting Anodes for Organic Solar Cells. *ACS Nano* **2012**, *6*, 5031–5039.
28. Kim, J.; Cote, L. J.; Kim, F.; Yuan, W.; Shull, K. R.; Huang, J. Graphene Oxide Sheets at Interfaces. *J. Am. Chem. Soc.* **2010**, *132*, 8180–8186.
29. Li, S.-S.; Tu, K.-H.; Lin, C.-C.; Chen, C.-W.; Chhowalla, M. Solution-Processable Graphene Oxide as an Efficient Hole Transport Layer in Polymer Solar Cells. *ACS Nano* **2010**, *4*, 3169–3174.
30. Pang, S.; Hernandez, Y.; Feng, X.; Müllen, K. Graphene as Transparent Electrode Material for Organic Electronics. *Adv. Mater.* **2011**, *23*, 2779–2795.
31. Park, H.; Brown, P. R.; Bulovic, V.; Kong, J. Graphene as Transparent Conducting Electrodes in Organic Photovoltaics: Studies in Graphene Morphology, Hole Transporting Layers, and Counter Electrodes. *Nano Lett.* **2012**, *12*, 133–140.
32. Wan, X.; Long, G.; Huang, L.; Chen, Y. Graphene—a Promising Material for Organic Photovoltaic Cells. *Adv. Mater.* **2011**, *23*, 5342–5358.
33. Yang, Z.; Chen, T.; He, R.; Guan, G.; Li, H.; Qiu, L.; Peng, H. Aligned Carbon Nanotube Sheets for the Electrodes of Organic Solar Cells. *Adv. Mater.* **2011**, *23*, 5436–5439.
34. Zhu, H.; Wei, J.; Wang, K.; Wu, D. Applications of Carbon Materials in Photovoltaic Solar Cells. *Sol. Energy Mater. Sol. Cells* **2009**, *93*, 1461–1470.
35. Rowell, M. W.; Topinka, M. A.; McGehee, M. D.; Prall, H.-J.; Dennler, G.; Sariciftci, N. S.; Hu, L.; Gruner, G. Organic Solar Cells with Carbon Nanotube Network Electrodes. *Appl. Phys. Lett.* **2006**, *88*, 233506.
36. Wang, X.; Zhi, L.; Tsao, N.; Tomović, Ž.; Li, J.; Müllen, K. Transparent Carbon Films as Electrodes in Organic Solar Cells. *Angew. Chem.* **2008**, *47*, 2990–2992.
37. Arranz-Andres, J.; Blau, W. J. Enhanced Device Performance Using Different Carbon Nanotube Types in Polymer Photovoltaic Devices. *Carbon* **2008**, *46*, 2067–2075.
38. Dillon, A. C. Carbon Nanotubes for Photoconversion and Electrical Energy Storage. *Chem. Rev.* **2010**, *110*, 6856–6872.
39. Geng, J.; Zeng, T. Influence of Single-Walled Carbon Nanotubes Induced Crystallinity Enhancement and Morphology Change on Polymer Photovoltaic Devices. *J. Am. Chem. Soc.* **2006**, *128*, 16827–16833.
40. Li, C.; Chen, Y.; Wang, Y.; Iqbal, Z.; Chhowalla, M.; Mitra, S. A Fullerene-Single Wall Carbon Nanotube Complex for Polymer Bulk Heterojunction Photovoltaic Cells. *J. Mater. Chem.* **2007**, *17*, 2406–2411.
41. Ren, S.; Bernardi, M.; Lunt, R. R.; Bulovic, V.; Grossman, J. C.; Gradecak, S. Toward Efficient Carbon Nanotube/P3HT Solar Cells: Active Layer Morphology, Electrical, and Optical Properties. *Nano Lett.* **2011**, *11*, 5316–5321.
42. Jia, Y.; Cao, A.; Bai, X.; Li, Z.; Zhang, L.; Guo, N.; Wei, J.; Wang, K.; Zhu, H.; Wu, D.; *et al*. Achieving High Efficiency Silicon-Carbon Nanotube Heterojunction Solar Cells by Acid Doping. *Nano Lett.* **2011**, *11*, 1901–1905.
43. Li, Z.; Kunets, V. P.; Saini, V.; Xu, Y.; Dervishi, E.; Salamo, G. J.; Biris, A. R.; Biris, A. S. Light-Harvesting Using High Density *p*-Type Single Wall Carbon Nanotube/*n*-Type Silicon Heterojunctions. *ACS Nano* **2009**, *3*, 1407–1414.
44. Landi, B. J.; Castro, S. L.; Ruf, H. J.; Evans, C. M.; Bailey, S. G.; Raffaelle, R. P. CdSe Quantum Dot-Single Wall Carbon Nanotube Complexes for Polymeric Solar Cells. *Sol. Energy Mater. Sol. Cells* **2005**, *87*, 733–746.
45. Arnold, M. S.; Zimmerman, J. D.; Renshaw, C. K.; Xu, X.; Lunt, R. R.; Austin, C. M.; Forrest, S. R. Broad Spectral Response Using Carbon Nanotube/Organic Semiconductor/C60 Photodetectors. *Nano Lett.* **2009**, *9*, 3354–3358.
46. Bindl, D. J.; Wu, M.-Y.; Prehn, F. C.; Arnold, M. S. Efficiently Harvesting Excitons from Electronic Type-Controlled Semiconducting Carbon Nanotube Films. *Nano Lett.* **2011**, *11*, 455–460.
47. Jain, R. M.; Howden, R.; Tvrdy, K.; Shimizu, S.; Hilmer, A. J.; McNicholas, T. P.; Gleason, K. K.; Strano, M. S. Polymer-Free near-Infrared Photovoltaics with Single Chirality (6,5) Semiconducting Carbon Nanotube Active Layers. *Adv. Mater.* **2012**, *24*, 4436–4439.
48. Tung, V. C.; Huang, J.-H.; Kim, J.; Smith, A. J.; Chu, C.-W.; Huang, J. Towards Solution Processed All-Carbon Solar Cells: A Perspective. *Energy Environ. Sci.* **2012**, *5*, 7810–7818.
49. Lee, H. W.; Yoon, Y.; Park, S.; Oh, J. H.; Hong, S.; Liyanage, L. S.; Wang, H.; Morishita, S.; Patil, N.; Park, Y. J.; *et al*. Selective Dispersion of High Purity Semiconducting Single-Walled Carbon Nanotubes with Regioregular Poly(3-Alkylthiophene)s. *Nat. Commun.* **2011**, *2*, 541.
50. Park, S.; Lee, H. W.; Wang, H.; Selvarasah, S.; Dokmeci, M. R.; Park, Y. J.; Cha, S. N.; Kim, J. M.; Bao, Z. Highly Effective Separation of Semiconducting Carbon Nanotubes Verified *via* Short-Channel Devices Fabricated Using Dip-Pen Nanolithography. *ACS Nano* **2012**, *6*, 2487–2496.
51. Yang, L.; Wang, S.; Zeng, Q.; Zhang, Z.; Pei, T.; Li, Y.; Peng, L.-M. Efficient Photovoltage Multiplication in Carbon Nanotubes. *Nat. Photonics* **2011**, *5*, 672–676.
52. Lemasson, F.; Berton, N.; Tittmann, J.; Hennrich, F.; Kappes, M. M.; Mayor, M. Polymer Library Comprising Fluorene and Carbazole Homo- and Copolymers for Selective Single-Walled Carbon Nanotubes Extraction. *Macromolecules* **2012**, *45*, 713–722.
53. Gerstel, P.; Klumpp, S.; Hennrich, F.; Altintas, O.; Eaton, T. R.; Mayor, M.; Barner-Kowollik, C.; Kappes, M. M. Selective Dispersion of Single-Walled Carbon Nanotubes *Via* Easily Accessible Conjugated Click Polymers. *Polym. Chem.* **2012**, *3*, 1966–1970.
54. Arnold, M. S.; Green, A. A.; Hulvat, J. F.; Stupp, S. I.; Hersam, M. C. Sorting Carbon Nanotubes by Electronic Structure Using Density Differentiation. *Nat. Nanotechnol.* **2006**, *1*, 60–65.
55. Bindl, D. J.; Safron, N. S.; Arnold, M. S. Dissociating Excitons Photogenerated in Semiconducting Carbon Nanotubes at

Polymeric Photovoltaic Heterojunction Interfaces. *ACS Nano* **2010**, *4*, 5657–5664.
56. Itkis, M. E.; Borondics, F.; Yu, A.; Haddon, R. C. Bolometric Infrared Photoresponse of Suspended Single-Walled Carbon Nanotube Films. *Science* **2006**, *312*, 413–416.
57. Hartschuh, A.; Pedrosa, H. N.; Peterson, J.; Huang, L.; Anger, P.; Qian, H.; Meixner, A. J.; Steiner, M.; Novotny, L.; Krauss, T. D. Single Carbon Nanotube Optical Spectroscopy. *ChemPhysChem* **2005**, *6*, 577–582.
58. Kataura, H.; Kumazawa, Y.; Maniwa, Y.; Umezu, I.; Suzuki, S.; Ohtsuka, Y.; Achiba, Y. Optical Properties of Single-Wall Carbon Nanotubes. *Synth. Met.* **1999**, *103*, 2555–2558.
59. Cognet, L.; Tsyboulski, D. A.; Rocha, J.-D. R.; Doyle, C. D.; Tour, J. M.; Weisman, R. B. Stepwise Quenching of Exciton Fluorescence in Carbon Nanotubes by Single-Molecule Reactions. *Science* **2007**, *316*, 1465–1468.
60. Luer, L.; Hoseinkhani, S.; Polli, D.; Crochet, J.; Hertel, T.; Lanzani, G. Size and Mobility of Excitons in (6, 5) Carbon Nanotubes. *Nat. Phys.* **2009**, *5*, 54–58.
61. Meshot, E. R.; Patel, K. D.; Tawfick, S.; Juggernauth, K. A.; Bedewy, M.; Verploegen, E. A.; De Volder, M. F. L.; Hart, A. J. Photoconductive Hybrid Films *Via* Directional Self-Assembly of C60 on Aligned Carbon Nanotubes. *Adv. Funct. Mater.* **2011**, *22*, 577–584.
62. Virkar, A.; Mannsfeld, S.; Oh, J. H.; Toney, M. F.; Tan, Y. H.; Liu, G.-y.; Scott, J. C.; Miller, R.; Bao, Z. The Role of Ots Density on Pentacene and C60 Nucleation, Thin Film Growth, and Transistor Performance. *Adv. Funct. Mater.* **2009**, *19*, 1962–1970.
63. Ramuz, M.; Burgi, L.; Winnewisser, C.; Seitz, P. High Sensitivity Organic Photodiodes with Low Dark Currents and Increased Lifetimes. *Org. Electron.* **2008**, *9*, 369–376.
64. Schuettfort, T.; Nish, A.; Nicholas, R. J. Observation of a Type II Heterojunction in a Highly Ordered Polymer−Carbon Nanotube Nanohybrid Structure. *Nano Lett.* **2009**, *9*, 3871–3876.
65. Kanai, Y.; Grossman, J. C. Role of Semiconducting and Metallic Tubes in P3HT/Carbon-Nanotube Photovoltaic Heterojunctions: Density Functional Theory Calculations. *Nano Lett.* **2008**, *8*, 908–912.
66. Hecht, D. S.; Hu, L.; Irvin, G. Emerging Transparent Electrodes Based on Thin Films of Carbon Nanotubes, Graphene, and Metallic Nanostructures. *Adv. Mater.* **2011**, *23*, 1482–1513.
67. Kumar, A.; Zhou, C. The Race to Replace Tin-Doped Indium Oxide: Which Material Will Win? *ACS Nano* **2010**, *4*, 11–14.
68. Gomez De Arco, L.; Zhang, Y.; Schlenker, C. W.; Ryu, K.; Thompson, M. E.; Zhou, C. Continuous, Highly Flexible, and Transparent Graphene Films by Chemical Vapor Deposition for Organic Photovoltaics. *ACS Nano* **2010**, *4*, 2865–2873.
69. Yin, Z.; Sun, S.; Salim, T.; Wu, S.; Huang, X.; He, Q.; Lam, Y. M.; Zhang, H. Organic Photovoltaic Devices Using Highly Flexible Reduced Graphene Oxide Films as Transparent Electrodes. *ACS Nano* **2010**, *4*, 5263–5268.
70. Wang, X.; Zhi, L.; Tsao, N.; Tomović, Ž.; Li, J.; Müllen, K. Transparent Carbon Films as Electrodes in Organic Solar Cells. *Angew. Chem.* **2008**, *120*, 3032–3034.
71. Wu, H.; Hu, L.; Rowell, M. W.; Kong, D.; Cha, J. J.; McDonough, J. R.; Zhu, J.; Yang, Y.; McGehee, M. D.; Cui, Y. Electrospun Metal Nanofiber Webs as High-Performance Transparent Electrode. *Nano Lett.* **2010**, *10*, 4242–4248.
72. Lee, J.-Y.; Connor, S. T.; Cui, Y.; Peumans, P. Solution-Processed Metal Nanowire Mesh Transparent Electrodes. *Nano Lett.* **2008**, *8*, 689–692.
73. Kang, M.-G.; Kim, M.-S.; Kim, J.; Guo, L. J. Organic Solar Cells Using Nanoimprinted Transparent Metal Electrodes. *Adv. Mater.* **2008**, *20*, 4408–4413.
74. Tvingstedt, K.; Inganäs, O. Electrode Grids for Ito Free Organic Photovoltaic Devices. *Adv. Mater.* **2007**, *19*, 2893–2897.
75. Vosgueritchian, M.; Lipomi, D. J.; Bao, Z. Highly Conductive and Transparent Pedot:Pss Films with a Fluorosurfactant for Stretchable and Flexible Transparent Electrodes. *Adv. Funct. Mater.* **2012**, *22*, 421–428.
76. Peh, R. J.; Lu, Y.; Zhao, F.; Lee, C.-L. K.; Kwan, W. L. Vacuum-Free Processed Transparent Inverted Organic Solar Cells with Spray-Coated Pedot:Pss Anode. *Sol. Energy Mater. Sol. Cells* **2011**, *95*, 3579–3584.
77. Kaltenbrunner, M.; White, M. S.; Glowacki, E. D.; Sekitani, T.; Someya, T.; Sariciftci, N. S.; Bauer, S. Ultrathin and Lightweight Organic Solar Cells with High Flexibility. *Nat. Commun.* **2012**, *3*, 770.
78. Zhou, Y.; Fuentes-Hernandez, C.; Shim, J.; Meyer, J.; Giordano, A. J.; Li, H.; Winget, P.; Papadopoulos, T.; Cheun, H.; Kim, J.; *et al*. A Universal Method to Produce Low-Work Function Electrodes for Organic Electronics. *Science* **2012**, *336*, 327–332.
79. Lipomi, D. J.; Tee, B. C. K.; Vosgueritchian, M.; Bao, Z. Stretchable Organic Solar Cells. *Adv. Mater.* **2011**, *23*, 1771–1775.
80. Lipomi, D. J.; Vosgueritchian, M.; Tee, B. C. K.; Hellstrom, S. L.; Lee, J. A.; Fox, C. H.; Bao, Z. Skin-Like Pressure and Strain Sensors Based on Transparent Elastic Films of Carbon Nanotubes. *Nat. Nanotechnol.* **2011**, *6*, 788–792.
81. Yamada, T.; Hayamizu, Y.; Yamamoto, Y.; Yomogida, Y.; Izadi-Najafabadi, A.; Futaba, D. N.; Hata, K. A Stretchable Carbon Nanotube Strain Sensor for Human-Motion Detection. *Nat. Nanotechnol.* **2011**, *6*, 296–301.
82. Kim, K. S.; Zhao, Y.; Jang, H.; Lee, S. Y.; Kim, J. M.; Kim, K. S.; Ahn, J.-H.; Kim, P.; Choi, J.-Y.; Hong, B. H. Large-Scale Pattern Growth of Graphene Films for Stretchable Transparent Electrodes. *Nature* **2009**, *457*, 706–710.
83. Liu, Z.; Li, J.; Sun, Z.-H.; Tai, G.; Lau, S.-P.; Yan, F. The Application of Highly Doped Single-Layer Graphene as the Top Electrodes of Semitransparent Organic Solar Cells. *ACS Nano* **2012**, *6*, 810–818.
84. Richard, R. L.; Vladimir, B. Transparent, near-Infrared Organic Photovoltaic Solar Cells for Window and Energy-Scavenging Applications. *Appl. Phys. Lett.* **2011**, *98*, 113305.
85. Lee, J.-Y.; Connor, S. T.; Cui, Y.; Peumans, P. Semitransparent Organic Photovoltaic Cells with Laminated Top Electrode. *Nano Lett.* **2010**, *10*, 1276–1279.
86. Huang, J.; Li, G.; Yang, Y. A Semi-Transparent Plastic Solar Cell Fabricated by a Lamination Process. *Adv. Mater.* **2008**, *20*, 415–419.
87. Gadisa, A.; Tvingstedt, K.; Admassie, S.; Lindell, L.; Crispin, X.; Andersson, M. R.; Salaneck, W. R.; Inganas, O. Transparent Polymer Cathode for Organic Photovoltaic Devices. *Synth. Met.* **2006**, *156*, 1102–1107.
88. Becerril, H. A.; Mao, J.; Liu, Z.; Stoltenberg, R. M.; Bao, Z.; Chen, Y. Evaluation of Solution-Processed Reduced Graphene Oxide Films as Transparent Conductors. *ACS Nano* **2008**, *2*, 463–470.
89. Hwang, J. O.; Park, J. S.; Choi, D. S.; Kim, J. Y.; Lee, S. H.; Lee, K. E.; Kim, Y.-H.; Song, M. H.; Yoo, S.; Kim, S. O. Work-function-Tunable, N-Doped Reduced Graphene Transparent Electrodes for High-Performance Polymer Light-Emitting Diodes. *ACS Nano* **2012**, *6*, 159–167.
90. Han, T.-H.; Lee, Y.; Choi, M.-R.; Woo, S.-H.; Bae, S.-H.; Hong, B. H.; Ahn, J.-H.; Lee, T.-W. Extremely Efficient Flexible Organic Light-Emitting Diodes with Modified Graphene Anode. *Nat. Photonics* **2012**, *6*, 105–110.
91. Liang, X.; Sperling, B. A.; Calizo, I.; Cheng, G.; Hacker, C. A.; Zhang, Q.; Obeng, Y.; Yan, K.; Peng, H.; Li, Q.; *et al*. Toward Clean and Crackless Transfer of Graphene. *ACS Nano* **2011**, *5*, 9144–9153.
92. Lin, Y.-C.; Lu, C.-C.; Yeh, C.-H.; Jin, C.; Suenaga, K.; Chiu, P.-W. Graphene Annealing: How Clean Can It Be? *Nano Lett.* **2012**, *12*, 414–419.
93. Yang, D.; Zhou, L.; Chen, L.; Zhao, B.; Zhang, J.; Li, C. Chemically Modified Graphene Oxides as a Hole Transport Layer in Organic Solar Cells. *Chem. Commun.* **2012**, *48*, 8078–8080.
94. Wei, P.; Oh, J. H.; Dong, G.; Bao, Z. Use of a 1*H*-Benzoimidazole Derivative as an *n*-Type Dopant and To Enable Air-Stable Solution-Processed *n*-Channel Organic Thin-Film Transistors. *J. Am. Chem. Soc.* **2010**, *132*, 8852–8853.
95. Wei, P.; Menke, T.; Naab, B. D.; Leo, K.; Riede, M.; Bao, Z. 2-(2-Methoxyphenyl)-1,3-dimethyl-1*H*-Bbenzoimidazol-3-ium

Iodide as a New Air-Stable n-Type Dopant for Vacuum-Processed Organic Semiconductor Thin Films. *J. Am. Chem. Soc.* **2012**, *134*, 3999–4002.
96. Koster, L. J. A.; Mihailetchi, V. D.; Ramaker, R.; Blom, P. W. M. Light Intensity Dependence of Open-Circuit Voltage of Polymer:Fullerene Solar Cells. *Appl. Phys. Lett.* **2005**, *86*, 123509.